





Dynamics of spontaneous wrapping of microparticles by floppy lipid membranes

Hendrik T. Spanke ¹, Jaime Agudo-Canalejo ², Daniel Tran ¹, Robert W. Style,¹ and Eric R. Dufresne ^{1,*}

¹Department of Materials, ETH Zürich, 8093 Zürich, Switzerland

²Max Planck Institute for Dynamics and Self-Organization (MPIDS), Am Faßberg 17, 37077 Göttingen, Germany



(Received 13 September 2021; accepted 13 April 2022; published 28 April 2022)

Lipid membranes form the barrier between the inside and outside of cells and many of their subcompartments. As such, they bind to a wide variety of nano- and micrometer sized objects and, in the presence of strong adhesive forces, strongly deform and envelop particles. This wrapping plays a key role in many healthy and disease-related processes. So far, little work has focused on the dynamics of wrapping. Here, using a model system of micron-sized colloidal particles and giant unilamellar lipid vesicles with tunable adhesive forces, we measure the velocity of the particle during wrapping as well as the forces exerted on it by the lipid membrane. Dissipation near the contact line appears to be the main factor determining the wrapping velocity and time to wrap an object.

DOI: [10.1103/PhysRevResearch.4.023080](https://doi.org/10.1103/PhysRevResearch.4.023080)

I. INTRODUCTION

Lipid membranes frequently come in contact with nano- and micro-objects. This is essential in many biological processes. Examples range from the disease-related entry of viruses and bacteria into cells [1,2] to healthy docking and priming during vesicular trafficking [3]. A large body of work has studied adhesive particle-membrane interactions [4–15]. However, only a few studies have focused on adhesion dynamics [16,17].

In theory, the interplay of a simple membrane with particles should be governed by only a few physical parameters. The membrane resists bending through its bending rigidity, κ_b , and stretching through its membrane tension, σ . Particle-membrane adhesion is characterized by the adhesion energy per unit area, ω . Above a critical adhesion energy, ω_c , a membrane will spontaneously wrap a particle coming into contact with it. For flat, tensionless membranes, $\omega_c = 2\kappa_b/R_p^2$, where R_p is the particle radius [18,19].

Here, we experimentally investigate the spontaneous wrapping of micron-sized particles by giant unilamellar vesicles (GUVs) in the biologically relevant limit of low membrane tension and weak reversible adhesion. We tune particle-membrane interactions using the depletion effect, and investigate how the wrapping dynamics change with increasing adhesion energy. Comparing spontaneous wrapping of free and optically trapped particles, we conclude that dissipation near the membrane-particle contact line controls the wrapping dynamics.

II. EXPERIMENTAL APPROACH

We use a recently developed model system consisting of a suspension of micron-sized polystyrene particles ($0.54 \pm 0.02 \mu\text{m}$ and $1.04 \pm 0.02 \mu\text{m}$ in radius) and GUVs ($9.8\text{--}24.6 \mu\text{m}$ in radius) combined with a depletant [18]. See Fig. 5 for a histogram of GUV sizes used. The GUVs are made by electroformation in a 280 mOsm/kg sucrose solution (see Sec. VI B for details). They consist of 1-palmitoyl-2-oleyl-sn-glycero-3-phosphocholine (POPC) with 1% 1,2-dioleoyl-sn-glycero-3-phosphoethanolamine-N-(lissamine rhodamine B sulfonyl) (rhodamine PE) [20–22]. We previously measured κ_b in this system to be $(33 \pm 8) k_B T$ [18].

The model system allows us to tune a number of parameters. We can vary ω by changing the concentration of polyethylene glycol (PEG) depletant. This has a molecular weight of 10^5 g/mol, a radius of gyration R_g of about 16 nm, and an overlap concentration of 0.99 wt. % [23,24]. We used PEG concentrations between 0.39–0.67 wt. % (± 0.016 wt. %). Steric repulsion due to strong thermal fluctuations of the membrane keep the particle and membrane at least 4–5 nm apart [25–27], yielding adhesion energy densities from 0.9–1.7 $\mu\text{J}/\text{m}^2$. Previous studies into the dynamics of particle wrapping consider much higher adhesion energy densities of $10^2\text{--}10^3 \mu\text{J}/\text{m}^2$ [16,17]. The osmolality of the outside solvent is adjusted through the addition of glucose (approximately 270 mM) to a slightly hypertonic value of 290 mOsm/kg. In addition to the PEG depletion agent, the solvent contains 10 mM of sodium chloride, screening electric charges and limiting the Debye length to 3 nm, and 0.05 wt. % of Pluronic F108 to passivate the surface of the particles. Over the course of hours, this slight osmotic imbalance drives the deflation of vesicles, leading to very low membrane tensions, $<10^{-9}$ N/m [18]. With these low membrane tensions, the adhesion energy driving the wrapping process is counteracted only by the bending energy of the membrane. Note that the

*eric.dufresne@mat.ethz.ch

Published by the American Physical Society under the terms of the Creative Commons Attribution 4.0 International license. Further distribution of this work must maintain attribution to the author(s) and the published article's title, journal citation, and DOI.

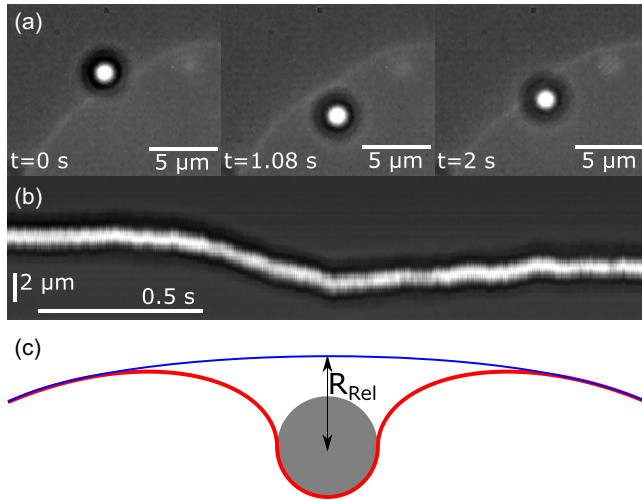


FIG. 1. Spontaneous wrapping. (a) Combined bright-field and fluorescence microscopy images of a PS particle $1.04 \mu\text{m}$ in radius being spontaneously wrapped by a POPC membrane in the presence of $0.67 \text{ wt. } \% \text{ PEG100K}$, corresponding to an adhesion energy of $1.7 \mu\text{J}/\text{m}^2$. (b) A kymograph showing the particle movement along an axis perpendicular to the membrane. (c) Schematic introducing the R_{Rel} coordinate. R_{Rel} expresses the shortest distance between the particle center and a parabola, fitted to the membrane outside of the immediate deformation caused by the particle.

bendocapillary length scale, $\lambda_\sigma = \sqrt{\kappa_b/\sigma}$, captures the relative importance of the bending rigidity and tension. When $R \ll \lambda_\sigma$, membrane tension is negligible and bending rigidity dominates [28]. This is true in the current system, where our particles are significantly smaller than $\lambda_\sigma > 10 \mu\text{m}$.

III. SPONTANEOUS WRAPPING OF FREE PARTICLES

Above a critical adhesion energy density, ω_c , a particle within range of the depletion interactions will be spontaneously engulfed by the membrane. The spontaneous wrapping process is presented in Fig. 1(a). Two acquired movies of the wrapping process can be found in the Supplementary Material [29]. The particle is observed to be quickly engulfed after being moved close to a GUV using an optical trap and coming into contact with the membrane. This process can be separated into two parts. At first, the particle moves about two particle radii toward the vesicle center. It reaches its furthest indentation after 1.08 seconds in the example shown in Fig. 1(a), before moving away from the vesicle center again and settling just underneath the membrane. During the whole process, the particle moves in a radial direction with respect to the GUV center. Figure 1(b) shows a kymograph along this perpendicular direction indicating the particle trajectory over time.

Wrapping of the particle is accompanied by movement of the particle as well as large-scale deformation of the membrane. Additionally, the membrane shows large thermal fluctuations with amplitudes on the order of μm , owing to the very low membrane tension [18]. For these reasons, we chose to express the wrapping progress through the position of the particle relative to the membrane, R_{Rel} , defined in Fig. 1(c). In experiments, the close-range deformation of the membrane induced by the particle cannot be resolved, Fig. 1(a). Outside

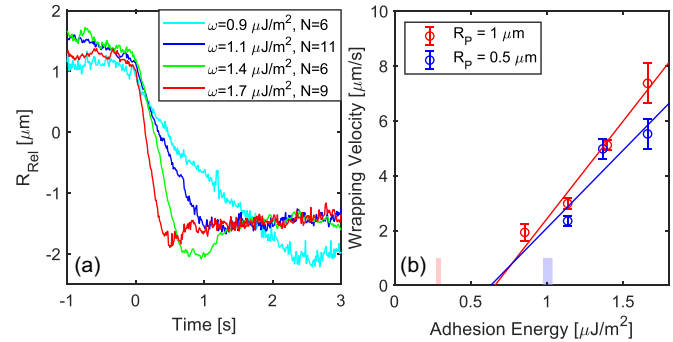


FIG. 2. Wrapping trajectories and velocities. (a) Averaged trajectories for a particle with a radius of $1.04 \mu\text{m}$ with increasing adhesion energy densities. Each curve is the average of N individual experiments, as is indicated in the legend. (b) Wrapping velocity as a function of adhesion energy density for particles with a radius of $1.04 \mu\text{m}$ in red and $0.54 \mu\text{m}$ in blue. Error bars indicate the standard errors. The fits are weighted by the number of experiments and show the trend for each particle size. The range of expected critical adhesion energy density for each particle size based on previous experiments [18] is indicated by the shaded area on the horizontal axis.

of the immediate vicinity of the particle, the membrane will return to an undisturbed shape. By fitting a parabola to this membrane segment, the undisturbed membrane at the particle position can be interpolated. We define R_{Rel} as the shortest distance between the tracked particle position and this parabola in each frame of the acquisition.

We imaged the wrapping process in samples with different adhesion energies, ω . Images were acquired at 1000 frames per second. The tracked position of the membrane was particularly susceptible to single-frame outliers, due to the low-light conditions at these high frame rates. The individual curves acquired were median-filtered over ten frames to remove this noise. Figure 2(a) shows R_{Rel} over time of $1.04 \mu\text{m}$ radius particles for four different adhesion energies ranging from 0.9 to $1.7 \mu\text{J}/\text{m}^2$. Each curve is the average of N individual experiments, as indicated in the legend. Averaged R_{Rel} trajectories for particles with a radius of $0.54 \mu\text{m}$ are shown in Fig. 7(a) in Appendix 4.

During the initial uptake, the slope of R_{Rel} versus time is approximately linear. Fitting these data for each individual experiment, we arrive at the wrapping velocities as a function of adhesion energy for particles with radii of $1.04 \mu\text{m}$ and $0.54 \mu\text{m}$ in Fig. 2(b). The observed wrapping velocities increase with adhesion energy, from about 2 to $8 \mu\text{m}/\text{s}$. Particle radius appears to have a weak effect on the wrapping velocities. Extrapolating the linear trend to much higher adhesion energy densities used in previous studies, we find wrapping velocities close to the reported values [17].

Note that we did not observe spontaneous wrapping for adhesion energy densities below 0.9 and $1.1 \mu\text{J}/\text{m}^2$ for the $1.04 \mu\text{m}$ and $0.54 \mu\text{m}$ particles, respectively. The onset of spontaneous wrapping is discontinuous due to an energy barrier separating the free and fully wrapped state [30]. Predicted values of the critical adhesion energy for spontaneous wrapping from [18] are consistent with the current data set and are indicated in Fig. 2(b).

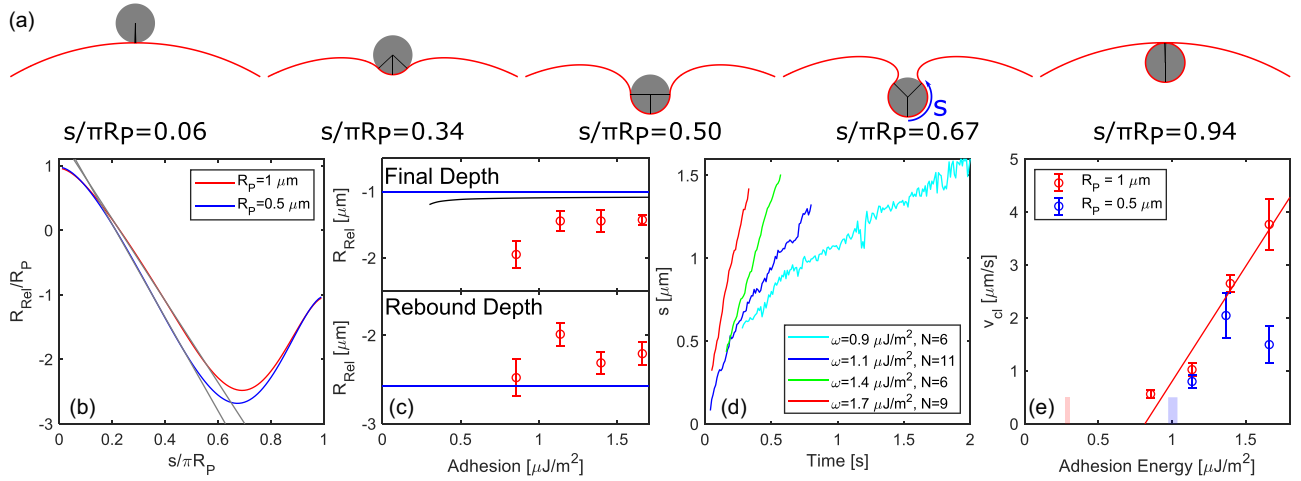


FIG. 3. Contact line velocity. (a) Quasistatic membrane shapes during the wrapping process for wrapping degrees (expressed by the arclength along the particle circumference in contact with the membrane) $s/\pi R_p$ of 0.06, 0.34, 0.50, 0.67, and 0.94 for a particle to vesicle radius ratio of 0.08. This ratio corresponds to a vesicle radius R_V of 13 μm , a typical size observed in experiments, and a particle radius R_p of 1.04 μm . The membrane is kept at the same level across schematics. (b) $R_{\text{Rel}}(s)$ for both particle to vesicle radius ratios of 0.08 and 0.04 corresponding to particle radii of 1.04 μm and 0.54 μm , respectively. $R_{\text{Rel}}(s)$ is normalized by the particle radius R_p and s by πR_p . Linear fits to the curves for values of s/R_p between 0.16 and 0.48 are also shown. The slopes of the linear fits are -2π and -2.3π for particles with radii of 1.04 μm and 0.54 μm , respectively. (c) The final R_{Rel} position at which the particle, $R_p = 1.04 \mu\text{m}$, settles after wrapping and the deepest indentation during the process. The error bars indicate the standard error. The blue line is the expected final position and deepest indentation of the particle from quasistatic models. The black line indicates $R_{\text{Rel}}(z)$, the expected average R_{Rel} position considering thermal fluctuations. (d) Arclength along the particle circumference $s(t)$ calculated from the averaged $R_{\text{Rel}}(t)$ trajectories shown in Fig. 2(a) for particles with $R_p = 1.04 \mu\text{m}$. (e) Contact line velocities from all experiments. The error bars indicate the standard error of the mean. The fit shown in red is weighted by the number of experiments and shows the trend for $R_p = 1.04 \mu\text{m}$. The range of expected critical adhesion energy density for each particle size based on previous experiments [18] is indicated by the shaded area on the horizontal axis.

To understand the shape of R_{Rel} over time we need to connect the shape of the membrane to the extent of wrapping. In previous experiments on this system, we found that membrane fluctuations with a wavelength on the order of 1 μm decay within 10^{-3} to 10^{-2} s [18]. Since the characteristic timescale of wrapping a particle of the same size is about one second, it seems reasonable to assume that the shape of the membrane in the vicinity of the particle is quasistatic. Following Appendix 1, we determined the membrane shape by minimizing the bending energy of the membrane, while fixing its contact area with the particle. Predicted membrane shapes for different contact areas are shown for $R_p/R_V = 0.08$ in Fig. 3(a). Here, we quantify the degree of wrapping as the arclength, s , from the bottom of the particle to the contact line. With these calculated membrane shapes, we can directly relate s to the observed relative position of the particle and membrane, R_{Rel} . As shown in Fig. 3(b), R_{Rel} initially decreases with s and reverses direction at $s/\pi R_p \approx 0.67$. Assuming that the wrapping process is quasistatic, the particle would settle at $R_{\text{Rel}} \approx -R_p$ after rebounding at $R_{\text{Rel}} \approx -2.5R_p$. In experiments, however, the final depth is deeper ($R_{\text{Rel}} \approx -1.5R_p$) and the rebound is more shallow than expected ($R_{\text{Rel}} \approx -2R_p$), as shown in Fig. 3(c). Thermal fluctuations of the particle partially account for the discrepancy in the final position, as shown by the black curve in Fig. 3(c), and described in Appendix 2.

Applying the quasistatic approximation throughout the wrapping process, we can replot $R_{\text{Rel}}(t)$ from Fig. 2(a) to show the time evolution of the extent of wrapping $s(t)$, shown in

Fig. 3(d). These trajectories, which include only data before the rebound, are quite linear, allowing us to estimate the contact line velocity, $v_{\text{cl}} = ds/dt$. The fitted values of v_{cl} for the full range of experimental conditions are plotted in Fig. 3(e). Note that the dependence of the contact line velocity with adhesion energy is qualitatively similar to that for the wrapping velocity [dR_{Rel}/dt , plotted in Fig. 2(b)]. However, the contact line velocities are about half the wrapping velocity. This makes sense, as $dR_{\text{Rel}}/ds \approx -2$ in the same stage of wrapping where dR_{Rel}/dt is constant [Fig. 3(b)].

In summary, the relative motion of the particle and membrane is largely consistent with a constant adhesion-dependent velocity of the contact line where the membrane comes into contact with the particle.

IV. SPONTANEOUS WRAPPING OF TRAPPED PARTICLES

To gain further insight into the dissipation pathways governing the wrapping process, we observe the wrapping of particles trapped in optical tweezers. We set the trap stiffness to 1.3–1.7 pN/ μm . In this regime, the particle displacements are small but resolvable, so that we can reliably measure forces. To completely wrap the particle, the membrane must therefore deform and translate as it engulfs the effectively stationary particle [Fig. 4(a)]. As shown in Fig. 4(b), the force on the particle increases at the onset of wrapping, and reaches its peak just as the particle becomes fully wrapped ($R_{\text{Rel}} = -R_p$). Afterward, the force slowly decays to zero as the vesicle relaxes to its equilibrium shape in the far-field. The

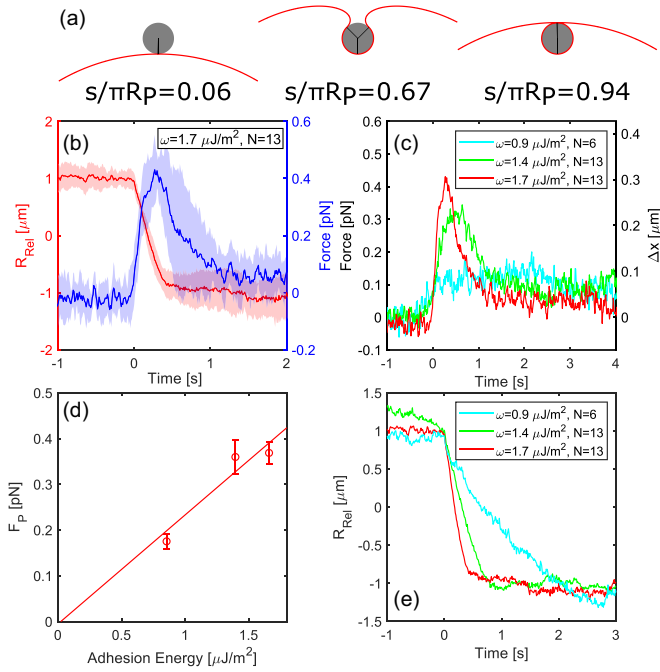


FIG. 4. Force measurement. (a) Quasistatic membrane shapes during the wrapping process (expressed by the arclength in contact with the membrane) $s/\pi R_p$ of 0.06, 0.67, and 0.94 for a particle to vesicle radius ratio of 0.08. This ratio corresponds to a vesicle radius R_V of 13 μm , a typical size observed in experiments, and a particle radius R_p of 1.04 μm . The particle is kept at the same level across schematics. (b) Averaged R_{Rel} and force for a particle with a radius of 1.04 μm at an adhesion energy density of 1.7 $\mu\text{J}/\text{m}^2$. (c) Averaged force for increasing adhesion energy densities ω . The displacements indicated on the right vertical axis correspond to the average trap stiffness, 1.4 $\text{pN}/\mu\text{m}$, of all experiments. (d) Peak force as a function of adhesion energy density for particles with a radius of 1.04 μm . The error bars indicate the standard error. The fit is weighted by the number of experiments and shows the trend. (e) Averaged R_{Rel} curves for increasing adhesion energy densities ω . Each curve is the average of N individual experiments, as is indicated in the legend.

peak forces, F_p , increase with the adhesion energy, as shown in Figs. 4(c) and 4(d). Peak values are in the range of 0.1 to 0.5 pN and increase with ω .

Interestingly, the relative motion of the particle and membrane is very similar for free [Fig. 2(a)] and trapped [Fig. 4(e)] particles. Specifically, the timescales of the wrapping processes are very similar, lasting just over a second for the highest adhesion energy in both experiments. This suggests that the dominant timescale depends on neither the relative motion of the particle and fluid nor the membrane and fluid. Instead, it is dominated by the relative motion of the particle and membrane. Indeed, the contact line velocities for the same particle size and adhesion energy are similar with and without the optical trap (see Fig. 6 in Appendix 3).

Previous theory considering a vesicle adhering to a flat and rigid substrate [31] predicted a contact line velocity,

$$v_{\text{cl}} = 0.24 \left(\frac{\omega h_0}{\eta \ell_D} \right), \quad (1)$$

where η is the bulk viscosity of the solvent. Since the particle and membrane are arbitrarily large in this model, the critical

adhesion energy vanishes, i.e., $\omega_c = 0$. The quantity ℓ_D is the width of the region near the contact line where dissipation takes place,

$$\ell_D = (2\kappa_b/\omega)^{1/4} h_0^{1/2}, \quad (2)$$

and h_0 is the equilibrium separation of the two surfaces. In our experiments, we expect $h_0 \approx 3.9\text{--}4.7$ nm [18,26], and the corresponding size of the dissipation zone to be $\ell_D = 30\text{--}40$ nm. This is much smaller than the radii of our particles. Therefore, we expect dissipation to be localized to a small region near the contact line where the membrane and particle meet.

For a system with finite particle and vesicle size, we have seen that wrapping only occurs above a critical adhesion energy, ω_c . Thus, we expect the contact line velocity to scale with $\omega - \omega_c$. Introducing a friction coefficient to the quasistatic model, we find

$$v_{\text{cl}} = \frac{\omega - \omega_c}{\eta_{\text{eff}}}. \quad (3)$$

See [19] and Appendix 1 for further discussion. Here, η_{eff} is an effective viscosity capturing the increased dissipation associated with the draining of fluid between the particle and membrane as they establish intimate contact [32,33].

Substituting $(\omega - \omega_c)$ for ω in Eq. (1), and comparing with Eq. (3) implies that $\eta_{\text{eff}} \approx 4.2(\eta \ell_D/h_0)$. Substituting in values from above, we find that η_{eff}/η is in the range of 30 to 40. Thus, with $\omega_c = 0.3$ $\mu\text{J}/\text{m}^2$ and the measured viscosity of the depletion media, $\eta = 1.9$ mPa s , we expect contact line velocities, v_{cl} , between 6 and 17 $\mu\text{m}/\text{s}$, about 4 to 10 times higher than measured in the experiments.

These theoretical predictions significantly overestimate the apparent speed of the contact line. This discrepancy could have many origins. For example, dissipation could drive departures of vesicle shape from the quasistatic model, leading to inaccurate determinations of the contact line speed. Alternatively, dissipation within the membrane could dominate over dissipation in the surrounding solvent. Comparing the bulk viscosity of the surrounding media and the membrane viscosity we can form a length scale η_m/η . Using a recently reported shear viscosity η_m of a POPC membrane, about 10 nPa s m , we find that this characteristic length scale is about 5 μm . We expect that the wrapping of objects much smaller than this length scale will be dominated by the membrane viscosity [34]. Using dimensional analysis, we estimate the velocity in that limit to be roughly $(\omega - \omega_c)R_p/\eta_m$. Unfortunately, this also overestimates the velocity by about a factor of ten. On the other hand, values of membrane viscosity are not firmly established and are expected to depend sensitively on the exact structure of the membrane [35,36].

V. CONCLUSION

We have characterized how wrapping dynamics change with increasing adhesion energy. As expected, higher adhesion leads to faster wrapping, but ultimately, the dynamics of wrapping by a floppy membrane appear to be controlled by dissipation at the contact line. As a consequence, wrapping velocities are largely independent of particle size, and so the time taken for an object to be wrapped is proportional to

the size of the object. Qualitatively, the shape of the uptake over time is captured by a quasistatic model. Nevertheless, significant quantitative deviations remain between theory and experiment.

Our micron-scale experiments have clear connections to the interactions of microplastics with living cells [37,38] as well as drug delivery pathways into cells. These experiments can be extended to study wrapping with nonspherical particles or tense membranes. The wrapping of nonspherical particles is significant for entry of certain pathogens into cells, such as the egg-shaped malaria parasite [2]. We expect that the dynamics of wrapping will change qualitatively when membranes are sufficiently tense for bending rigidity to be negligible, i.e., $R \gg \lambda_\sigma$. In this limit, analogies with adhesion of particles to liquid-liquid interfaces may prove powerful. In that context, previous experimental results are available both for spheres [39] and ellipsoids [40]. Exploring model systems in these regimes will help to establish the physical foundations for an understanding of membrane-particle interactions over a wide range of scales.

VI. MATERIALS AND METHODS

A. Materials

1-palmitoyl-2-oleoyl-sn-glycero-3-phosphocholine (POPC) and 1,2-dioleoyl-sn-glycero-3-phosphoethanolamine-N-(lissamine rhodamine B sulfonyl) (ammonium salt) (Rh-DOPE) were purchased from Avanti Polar Lipids, Inc. (Alabaster, Alabama). D-(+)-glucose (BioXtra, $\geq 99.5\%$) and sucrose (BioXtra, $\geq 99.5\%$) were purchased from Sigma Life Science. NaCl (ACS reagent, $\geq 99.0\%$), poly(ethylene glycol) diacrylate with an average molecular weight $M_n = 700$, and chloroform were bought from Sigma-Aldrich. Ethanol, absolute, was purchased from Fisher Chemicals. 3-(trimethoxysilyl)propyl methacrylate was purchased from TCI (Tokyo Chemical Industry). Poly(ethylene oxide) (also called polyethylene glycol, PEG) powder with average M_v of 100 000, 2-hydroxy-4'-(2-hydroxyethoxy)-2-methylpropiophenone (Irgacure 2959), as well as poly(ethylene glycol)-block-poly(propylene glycol)-block-poly(ethylene glycol) (PEG-PPG-PEG, Pluronic F108, average $M_n \sim 14\,600$) were bought from Aldrich Chemistry. Fluorescent polystyrene particles with a diameter of $1.08\ \mu\text{m}$ and $2.07\ \mu\text{m}$ were purchased from Microparticles GmbH (Berlin, Germany).

All chemicals were used as received.

B. Electroformation of GUVs

POPC was used to make giant unilamellar vesicles by electroformation [20,21]. Rhodamine tagged lipids (Rh-DOPE) are added in the low concentration of 1%. $50\ \mu\text{L}$ of a 1 mM solution of these lipids was deposited on two platinum wires 5 mm apart using a glass syringe (Hamilton). The two wires are part of a PTFE chamber which is filled with a solution of 280 mOsm/kg sucrose and sealed with parafilm-covered PMMA windows. Both wires are connected electrically to a signal generator (Keysight 33210A). The electroformation protocol consists of gentle increase in AC voltage over 25 minutes from 0 to 5 V with a fixed frequency of 10 Hz. After

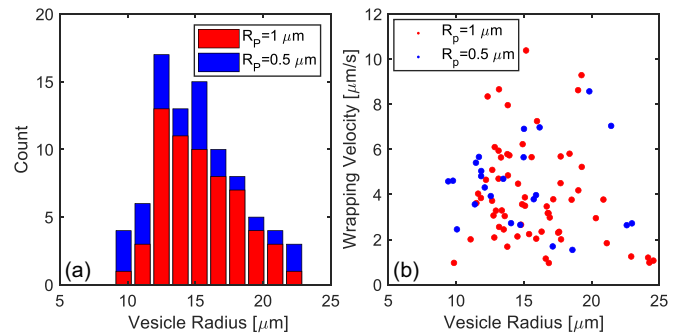


FIG. 5. Vesicle size. (a) Histogram of vesicle radii R_V . GUVs wrapping 1.04 and $0.54\ \mu\text{m}$ radii particles are indicated in red and blue, respectively. (b) Wrapping velocity for each experiment versus the vesicle radius. GUVs wrapping 1.04 and $0.54\ \mu\text{m}$ radii particles are indicated in red and blue, respectively.

the voltage reaches 5 V it is left for two hours. The frequency is then lowered to 5 Hz for another 30 minutes. Vesicles with varying sizes between a few μm and up to $50\ \mu\text{m}$ are taken out and stored in the 280 mM sucrose solution from the chamber at $4\ ^\circ\text{C}$ where they are stable for up to a few weeks.

C. Experimental procedure

The samples were prepared as is described in [18]. The substrate was covered in a thin layer of PEG-DA hydrogel preventing the GUVs from bursting as they settle. An imaging spacer (Grace Bio-Labs SecureSeal imaging spacer purchased through Sigma-Aldrich) was placed on the hydrogel-coated substrate. The sample volume was then filled with $70\ \mu\text{L}$ depletion medium, 0.3 to $0.5\ \mu\text{L}$ of a $0.025\ \text{wt.}\%$ particle suspension, and $10\ \mu\text{L}$ sucrose solution containing the GUVs before sealing it.

D. Optical microscopy and micromanipulation

Experiments using optical tweezers were done with Nikon Ti Eclipse inverted microscopes using a $60\times$ water immersion objective lens. Videos were taken at 1000 frames per second with a Hamamatsu ORCA-Flash 4.0, C13440. The trapping laser was a LUXX 785-200 laser from Omicron Laserage Laserprodukte GmbH with a wavelength of 785 nm and a maximum power of 200 mW. The initially vertically polarized laser is sent through a half-wave plate and a polarizing beamsplitter. By correctly orienting the half-wave plate it is possible to tune the laser power entering the sample while keeping the laser output constant. Behind the beamsplitter the still linearly polarized laser beam is circularized by a quarter-wave plate. The optical trap stiffness was calibrated passively using the equipartition theorem and Boltzmann statistics method described in [41]. The stiffnesses were measured to be between 1.3 and $1.7\ \text{pN}/\mu\text{m}$.

All GUVs used for experiments had negligible membrane tension. This was shown in a previous paper using the exact same system [18]. We defined the vesicle radius R_V as the average of major and minor axis. All vesicles used for experiments were between 9.8 and $24.6\ \mu\text{m}$ in radius. Figure 5(a) shows a histogram of vesicle sizes. We did not observe a

correlation between vesicle size and wrapping velocity, as can be seen in Fig. 5(b).

ACKNOWLEDGMENTS

We acknowledge helpful conversations with Jan Vermant as well as funding from Grant No. 172824 of the Swiss National Science Foundation.

APPENDIX

1. Quasistatic model

The membrane will conform to the particle curvature as it wraps around the particle. A degree of wrapping, q , can be defined as the fraction of the particle surface area bound to the membrane [42]. The distance z between the bottom of the particle and the contact line is then given by $z = 2R_p q$. The membrane is taken to be part of a vesicle with constant area A_V and variable enclosed volume, so that in the absence of the particle it forms a sphere with radius $R_V = \sqrt{A_V/4\pi}$. The equilibrium shapes of the membrane can be calculated for different levels of wrapping. They are calculated numerically by solving the membrane shape equations using a shooting method [43,44].

The energy of a small particle in contact with a much larger vesicle with local mean curvature M and spontaneous curvature m can be written as [42]

$$E(q) = 16\pi\kappa_b R_p [(m - M_{co})q + (M - m)q(1 - q)], \quad (\text{A1})$$

where κ_b is the bending rigidity and

$$M_{co} \equiv \sqrt{\frac{\omega}{2\kappa_b}} - \frac{1}{R_p}. \quad (\text{A2})$$

In this notation the condition for spontaneous wrapping is simply $M_{co} = M$. For small particles Eq. (A2) can be rewritten as

$$\frac{\omega R_p^2}{2\kappa_b} \approx 1 + 2M_{co} R_p. \quad (\text{A3})$$

Similarly, from the condition for spontaneous wrapping, we can write the critical adhesion ω_c for spontaneous wrapping as

$$\frac{\omega_c R_p^2}{2\kappa_b} \approx 1 + 2M R_p. \quad (\text{A4})$$

Making all these replacements in (A1), ignoring spontaneous curvature $m = 0$ [18], and taking $M = 1/R_V$, the vesicle curvature, we can rewrite the energy as

$$E(z) = -8\pi\kappa_b \left[\frac{(\omega - \omega_c) R_p^2}{2\kappa_b} \frac{z}{2R_p} + 2 \frac{R_p}{R_V} \left(\frac{z}{2R_p} \right)^2 \right]. \quad (\text{A5})$$

$E(z)$ has a parabolic shape as a function of z , and as expected the free state becomes unstable when $\omega = \omega_c$.

For adhesion energies much larger than ω_c , so that $(\omega - \omega_c) \gg \kappa_b/R_p R_V$, this simplifies to

$$E(z) = -2\pi R_p (\omega - \omega_c) z. \quad (\text{A6})$$

We note that this can also be written as a function of arclength s , using $z = R_p[1 - \cos(s/R_p)]$, which gives

$$E(s) = -2\pi R_p^2 (\omega - \omega_c) [1 - \cos(s/R_p)]. \quad (\text{A7})$$

We now consider overdamped dynamics of this contact line arclength [19]:

$$\dot{s} = \frac{1}{\xi(s)} E'(s) = \frac{1}{\xi(s)} 2\pi R_p (\omega - \omega_c) \sin(s/R_p), \quad (\text{A8})$$

where $\xi(s)$ is a friction coefficient, in principle dependent on the arclength. The circumference of the contact line is given by $L_{co}(s) = 2R_p \sin(s/R_p)$. If we assume that friction is proportional to L_{co} as $\xi(s) = \eta_{\text{eff}} L_{co}(s)$, with η_{eff} an effective viscosity, then Eq. (A8) becomes

$$\dot{s} = \frac{\omega - \omega_c}{\eta_{\text{eff}}}. \quad (\text{A9})$$

That is, we predict that the velocity of the contact line arclength is constant (independent of s and the particle radius R_p).

2. Impact of thermal fluctuations on final particle position

Thermal fluctuations of the particle could account for only part of discrepancies in the final particle depth. In equilibrium, the average distance, z , between the bottom of the particle and the contact line in the perpendicular direction to the undisturbed membrane, is given by the Boltzmann distribution

$$\langle z \rangle = \frac{\int_0^{2R_p} z e^{-E(z)/k_B T} dz}{\int_0^{2R_p} e^{-E(z)/k_B T} dz}. \quad (\text{A10})$$

Here, $E(z)$ is the energy of the membrane-particle system, given in Eq. (A5). The wrapping depth z is related to the arclength s through $z = R_p[1 - \cos(s/R_p)]$. The black line in Fig. 3(c) shows $R_{\text{rel}}(z)$ as a function of the adhesion energy density ω . While the particle's thermal fluctuations increase the expected resting depth, they account for only a small part of the deviation between the experiment and quasistatic model. In addition, the depletion interactions which bind particles to the membrane also favor adhesion of the membrane to itself. This could drive extension of the narrow neck connecting the fully wrapped particle to the rest of the membrane.

3. Contact line velocity of free and trapped particle

Figure 6 shows the averaged contact line velocities of all experiments with particles with a radius $R_p = 1.04 \mu\text{m}$. The red and blue data indicate experiments with a free and trapped particles, respectively.

4. Impact of particle size

Figure 7(a) shows R_{rel} over time for three different adhesion energy densities ranging from 1.1 to 1.7 $\mu\text{J}/\text{m}^2$. Each curve is the average of N individual experiments, as is indicated in the legend. Before averaging, the individual curves were median-filtered over ten frames to filter out noise.

Figure 7(b) shows the extracted $s(t)$ from the averaged $R_{\text{rel}}(t)$ trajectories shown in Fig. 2(a). A modeled R_{rel} curve

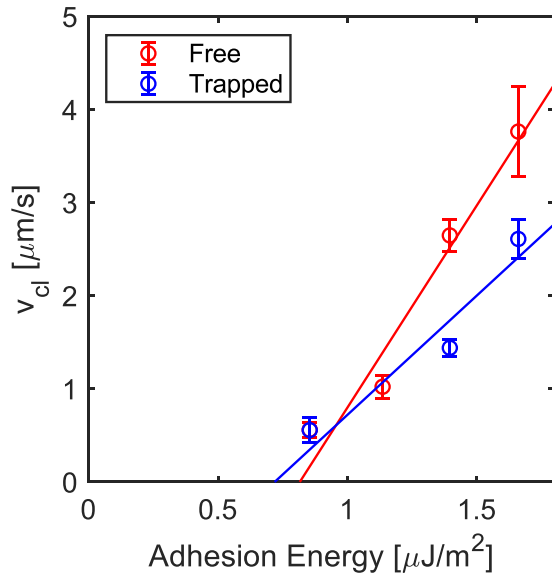


FIG. 6. Contact line velocity of trapped particle. Contact line velocities of all free and trapped particle experiments with $R_p = 1.04 \mu\text{m}$. The error bars indicate the standard error of the mean. The fits are weighted by the number of experiments and show the trend.

for a particle with a radius of $0.54 \mu\text{m}$ at an adhesion energy density of $1.7 \mu\text{J}/\text{m}^2$ is shown in Fig. 7(d) in blue. The average R_{Rel} curve from experiments is shown in black. An error for each time point is indicated by the area shaded in red. The contact line velocity used to obtain the blue curve is $v_{\text{cl}} = 2.75 \mu\text{m}/\text{s}$ (chosen to fit the data). As discussed in the main text the depth at which the particle settles after the wrapping process will be at $R_{\text{Rel}} = -R_p$ and the rebound depth, or the deepest indentation of the particle into the membrane will be at $R_{\text{Rel}} \approx -2.5R_p$. These two R_{Rel} coordinates will not change

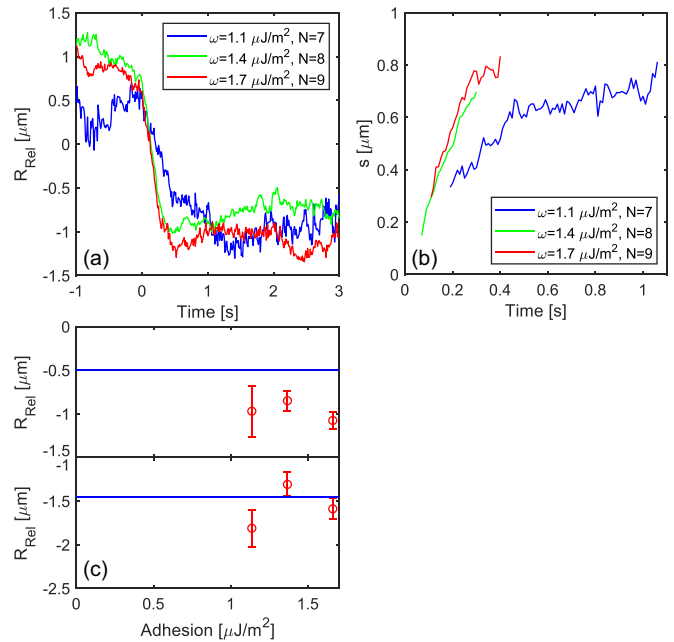


FIG. 7. Effect of particle size. (a) Averaged R_{Rel} curves for a particle with a radius of $0.54 \mu\text{m}$ with increasing adhesion energy densities. Each curve is the average of N individual experiments, as is indicated in the legend. (b) Arclength along the particle circumference $s(t)$ calculated from the averaged $R_{\text{Rel}}(t)$ trajectories shown in (a). (c) The final R_{Rel} position at which the particle settles after wrapping and the deepest indentation during the process. The error bars indicate the standard error. The blue line is the expected final position and deepest indentation of the particle from quasistatic models.

with changing adhesion energy density. In experiments we still consistently see lower final depths although the deepest indentation is observed to match with the quasistatic model as is visible in Fig. 7(c).

- [1] R. S. Flannagan, V. Jaumouill e, and S. Grinstein, The cell biology of phagocytosis, *Annu. Rev. Pathol.: Mech. Dis.* **7**, 61 (2012).
- [2] S. Dasgupta, T. Auth, N. S. Gov, T. J. Satchwell, E. Hanssen, E. S. Zuccala, D. T. Riglar, A. M. Toye, T. Betz, J. Baum, and G. Gompper, Membrane-wrapping contributions to malaria parasite invasion of the human erythrocyte, *Biophys. J.* **107**, 43 (2014).
- [3] T. S udhof, Neurotransmitter release: The last millisecond in the life of a synaptic vesicle, *Neuron* **80**, 675 (2013).
- [4] R. Lipowsky and H.-G. D obereiner, Vesicles in contact with nanoparticles and colloids, *Europhys. Lett.* **43**, 219 (1998).
- [5] A. H. Bahrami, M. Raatz, J. Agudo-Canalejo, R. Michel, E. M. Curtis, C. K. Hall, M. Gradzielski, R. Lipowsky, and T. R. Weikl, Wrapping of nanoparticles by membranes, *Adv. Colloid Interface Sci.* **208**, 214 (2014).
- [6] S. Dasgupta, T. Auth, and G. Gompper, Shape and orientation matter for the cellular uptake of nonspherical particles, *Nano Lett.* **14**, 687 (2014).
- [7] B. J. Reynwar, G. Illya, V. A. Harmandaris, M. M. M uller, K. Kremer, and M. Deserno, Aggregation and vesiculation of membrane proteins by curvature-mediated interactions, *Nature (London)* **447**, 461 (2007).
- [8] A. H. Bahrami, R. Lipowsky, and T. R. Weikl, Tubulation and Aggregation of Spherical Nanoparticles Adsorbed on Vesicles, *Phys. Rev. Lett.* **109**, 188102 (2012).
- [9] M. Raatz, R. Lipowsky, and T. R. Weikl, Cooperative wrapping of nanoparticles by membrane tubes, *Soft Matter* **10**, 3570 (2014).
- [10] K. Xiong, J. Zhao, D. Yang, Q. Cheng, J. Wang, and H. Ji, Cooperative wrapping of nanoparticles of various sizes and shapes by lipid membranes, *Soft Matter* **13**, 4644 (2017).
- [11] I. Koltover, J. O. R adler, and C. R. Safinya, Membrane Mediated Attraction and Ordered Aggregation of Colloidal Particles Bound to Giant Phospholipid Vesicles, *Phys. Rev. Lett.* **82**, 1991 (1999).
- [12] T. Ruiz-Herrero, E. Velasco, and M. F. Hagan, Mechanisms of budding of nanoscale particles through lipid bilayers, *J. Phys. Chem. B* **116**, 9595 (2012).

- [13] A. Šarić and A. Cacciuto, Fluid Membranes Can Drive Linear Aggregation of Adsorbed Spherical Nanoparticles, *Phys. Rev. Lett.* **108**, 118101 (2012).
- [14] A. Šarić and A. Cacciuto, Self-assembly of nanoparticles adsorbed on fluid and elastic membranes, *Soft Matter* **9**, 6677 (2013).
- [15] A. Vahid, A. Šarić, and T. Idema, Curvature variation controls particle aggregation on fluid vesicles, *Soft Matter* **13**, 4924 (2017).
- [16] S. Mirigian and M. Muthukumar, Kinetics of particle wrapping by a vesicle, *J. Chem. Phys.* **139**, 044908 (2013).
- [17] C. Dietrich, M. Angelova, and B. Pouligny, Adhesion of latex spheres to giant phospholipid vesicles: Statics and dynamics, *J. Phys. II* **7**, 1651 (1997).
- [18] H. T. Spanke, R. W. Style, C. François-Martin, M. Feofilova, M. Eisentraut, H. Kress, J. Agudo-Canalejo, and E. R. Dufresne, Wrapping of Microparticles by Floppy Lipid Vesicles, *Phys. Rev. Lett.* **125**, 198102 (2020).
- [19] J. Agudo-Canalejo and R. Lipowsky, Critical particle sizes for the engulfment of nanoparticles by membranes and vesicles with bilayer asymmetry, *ACS Nano* **9**, 3704 (2015).
- [20] M. I. Angelova and D. S. Dimitrov, Liposome electroformation, *Faraday Discuss. Chem. Soc.* **81**, 303 (1986).
- [21] M. I. Angelova, S. Soléau, P. Méléard, F. Faucon, and P. Bothorel, Preparation of giant vesicles by external AC electric fields: Kinetics and applications, in *Trends in Colloid and Interface Science VI*, edited by C. Helm (Steinkopff, Darmstadt, 1992), pp. 127–131.
- [22] R. Dimova and C. Marques, *The Giant Vesicle Book* (CRC Press, 2019).
- [23] N. Ziębacz, S. A. Wieczorek, T. Kalwarczyk, M. Fiałkowski, and R. Hołyst, Crossover regime for the diffusion of nanoparticles in polyethylene glycol solutions: Influence of the depletion layer, *Soft Matter* **7**, 7181 (2011).
- [24] M. Rubinstein and R. H. Colby, *Polymer Physics* (Oxford University Press, New York, 2003).
- [25] W. Helfrich, Steric interaction of fluid membranes in multilayer systems, *Z. Naturforsch., A: Phys. Sci.* **33**, 305 (1978).
- [26] W. Helfrich and R. M. Servuss, Undulations, steric interaction and cohesion of fluid membranes, *Nuovo Cimento D* **3**, 137 (1984).
- [27] W. Janke, H. Kleinert, and M. Meinert, Monte Carlo study of a stack of self-avoiding surfaces with extrinsic curvature stiffness, *Phys. Lett. B* **217**, 525 (1989).
- [28] M. Deserno, Elastic deformation of a fluid membrane upon colloid binding, *Phys. Rev. E* **69**, 031903 (2004).
- [29] See Supplemental Material <http://link.aps.org/supplemental/10.1103/PhysRevResearch.4.023080> for the raw data of Figs. 2(b), 4(d) and 5, and two movies showing a free and trapped particle being spontaneously wrapped by a lipid membrane.
- [30] M. Deserno, When do fluid membranes engulf sticky colloids?, *J. Phys.: Condens. Matter* **16**, S2061 (2004).
- [31] M. J. Blount, M. J. Miksis, and S. H. Davis, Thin-film flow beneath a vesicle during adhesion processes, *Procedia IUTAM* **16**, 33 (2015).
- [32] I. Cantat, K. Kassner, and C. Misbah, Vesicles in haptotaxis with hydrodynamical dissipation, *Eur. Phys. J. E* **10**, 175 (2003).
- [33] A.-L. Bernard, M.-A. Guedeau-Boudeville, L. Jullien, and J.-M. di Meglio, Strong adhesion of giant vesicles on surfaces: Dynamics and permeability, *Langmuir* **16**, 6809 (2000).
- [34] M. Arroyo and A. DeSimone, Relaxation dynamics of fluid membranes, *Phys. Rev. E* **79**, 031915 (2009).
- [35] B. A. Camley, C. Esposito, T. Baumgart, and F. L. Brown, Lipid bilayer domain fluctuations as a probe of membrane viscosity, *Biophys. J.* **99**, L44 (2010).
- [36] T. T. Hormel, S. Q. Kurihara, M. K. Brennan, M. C. Wozniak, and R. Parthasarathy, Measuring Lipid Membrane Viscosity Using Rotational and Translational Probe Diffusion, *Phys. Rev. Lett.* **112**, 188101 (2014).
- [37] M. A. Browne, A. Dissanayake, T. S. Galloway, D. M. Lowe, and R. C. Thompson, Ingested microscopic plastic translocates to the circulatory system of the mussel, *Mytilus edulis* (L.), *Environ. Sci. Technol.* **42**, 5026 (2008).
- [38] N. von Moos, P. Burkhardt-Holm, and A. Köhler, Uptake and effects of microplastics on cells and tissue of the blue mussel *Mytilus edulis* L. after an experimental exposure, *Environ. Sci. Technol.* **46**, 11327 (2012).
- [39] A. Wang, R. McGorty, D. M. Kaz, and V. N. Manoharan, Contact-line pinning controls how quickly colloidal particles equilibrate with liquid interfaces, *Soft Matter* **12**, 8958 (2016).
- [40] S. Coertjens, R. D. Dier, P. Moldenaers, L. Isa, and J. Vermant, Adsorption of ellipsoidal particles at liquid–liquid interfaces, *Langmuir* **33**, 2689 (2017).
- [41] M. Sarshar, W. Wong, and B. Anvari, Comparative study of methods to calibrate the stiffness of a single-beam gradient-force optical tweezers over various laser trapping powers, *J. Biomed. Opt.* **19**, 115001 (2014).
- [42] J. Agudo-Canalejo and R. Lipowsky, Uniform and Janus-like nanoparticles in contact with vesicles: Energy landscapes and curvature-induced forces, *Soft Matter* **13**, 2155 (2017).
- [43] U. Seifert, K. Berndl, and R. Lipowsky, Shape transformations of vesicles: Phase diagram for spontaneous-curvature and bilayer-coupling models, *Phys. Rev. A* **44**, 1182 (1991).
- [44] J. Agudo-Canalejo and R. Lipowsky, Stabilization of membrane necks by adhesive particles, substrate surfaces, and constriction forces, *Soft Matter* **12**, 8155 (2016).